# Title: Bacterial DNA on the skin surface overrepresents the viable skin microbiome

**Authors:** Ellen M Acosta[1], Katherine A Little[1], Benjamin P Bratton[1,2], Xuming Mao[3], Aimee Payne[3], Danelle Devenport[1], Zemer Gitai[1*]

**Affiliations:**

[1] Department of Molecular Biology, Princeton University, Princeton, NJ 08544, USA.

[2] Lewis-Sigler Institute for Integrative Genomics, Princeton University, Princeton, NJ 08544, USA.

[3]Department of Dermatology, University of Pennsylvania, Philadelphia, PA 19104, USA.

*Correspondence to: zgitai@princeton.edu

**Abstract:** The skin microbiome provides vital contributions to human health and was historically assumed to be a well-mixed community that coats the skin surface. However, its spatial organization and viability remain unclear. Here we apply culturing, imaging, and molecular approaches to both human and mouse skin samples, and find that the skin surface is colonized by far few viable bacteria than would be predicted by its levels of bacterial DNA. Instead, viable skin-associated bacteria are primarily present in hair follicles and other cutaneous invaginations. Furthermore, we establish that a relatively small number of bacterial families dominate each skin site and that traditional sequencing methods overestimate the skin microbiome's richness and diversity. These findings address multiple outstanding questions in skin microbiome biology with significant implications for future efforts to study and manipulate it.

**Main Text:** The skin is the largest organ in the human body, providing roughly 25 square meters for potential host-microbe interactions (*1*). It facilitates our tactile interactions with the world, separates us from the dangers of our daily lives, and has the incredible ability to regenerate itself every 20-30 days (*2*). Human skin is also home to the organisms that comprise the skin microbiome, which has been shown to have important roles in human health. For example, the human skin microbiome affects immune system education (*3*, *4*), wound healing (*5*–*7*), colonization resistance (*8*), modulation of gene expression in the skin (*9*), and may have a role in development (*10*). Despite the important contributions of the skin microbiome to human health, there are important questions that have not been addressed by traditional methods: Why is the skin microbiome stable across months in longitudinal studies yet easily perturbed upon transient environmental changes like swimming (*11*)? Why are there so many anaerobic bacteria on an organ exposed to the air? How can the microbes educate immune cells that are not found on the surface? And why is it so difficult to stably colonize the skin with new microbes without strong perturbations like abrasion?

The skin microbiome is often depicted as a well-mixed coating of microbes on the skin surface (*12*, *13*). This assumption underlies both the paradoxes in the field mentioned above and the predominant method by which skin microbiomes have been studied: sequencing of swabbed skin areas (*14*). Additionally, while sequencing and culture-based studies have demonstrated that bacteria extend into deeper portions of the skin, the spatial distribution of the skin microbiome as a whole has not been well characterized (*4*, *15*, *16*). To address this gap, we determined the spatial distribution of bacterial cells in the skin using the universal bacterial FISH probe EUB338, which hybridizes to bacterial 16S rRNA (*17*). Using this method on biopsied healthy adult human tissues revealed that the skin surface contains very few intact bacteria (Fig.1 A). In

contrast, clusters of bacteria were found within hair follicles and other cutaneous skin structures like comedos (Fig.1 B). To quantify these observations, we calculated the ratio of the mean fluorescence within an area of interest (a hair follicle, the skin surface, or other cutaneous structures) to the mean fluorescence outside of the area of interest. We refer to this ratio as an enrichment score. The median enrichment score for human follicles was 11.24 (Fig. 1 D). In contrast, the skin surface (stratum corneum) had an enrichment score of just 0.188. This pattern of observing many bacteria in follicles but few on the skin surface held true when using FISH probes specific for *Cutibacterium acnes*, one of the most abundant bacterial species in the human skin microbiome (Fig. 1 C). For *C. acnes*, the enrichment score was 3.14 for follicles as compared to 0.67 for the stratum corneum (Fig. 1 D). We note that while the vast majority of intact skin-associated bacteria were not associated with the skin surface, there were some bacteria present in the stratum corneum. Thus, our results are consistent with previous reports that bacteria can be cultured from skin surface swabs but also extend these findings to demonstrate that the skin surface has fewer intact bacteria than deeper skin structures.

DNA sequencing of samples collected by sterile swabbing is the most common method used to evaluate the skin microbiome because it is simple, noninvasive, and has been shown to result in higher consistency than other sampling methods (*18*). However, because we observed so few bacterial cells on the skin surface, we questioned whether the bacterial DNA that is present on the skin surface and accessible for sampling by swabs is representative of the viable microbiome. We thus implemented a method that allowed us to quantify and compare total bacterial DNA with bacterial DNA found only within viable bacterial cells. Specifically, we utilized the cell-impermeable small molecule propidium monoazide (PMA), which binds irreversibly to double-stranded DNA upon photoactivation to inhibit PCR amplification (Fig. 2

A) (*19*). When PMA photoactivation is performed before the cell lysis step of DNA isolation, the genomic DNA inside viable bacteria is protected from PMA binding because PMA is cell-impermeable, while cell-free DNA or DNA within permeabilized bacteria becomes PMA-bound. Thus, comparing DNA quantities in samples with and without PMA treatment enables assessment of the viability of a bacterial population. This approach was previously used to assess the viability of bacteria from environmental waste water samples (*20*). To quantify bacterial DNA and assess the viability of a population of cells, we combined the use of PMA with droplet digital PCR (PMA-ddPCR).

To assure that PMA-ddPCR would allow us to reliably gauge the fraction of viable cells in a population, we first validated that it generated the expected results using known ratios of heat-killed and exponentially-growing *E. coli* cultures (Fig. S1A). As a further demonstration that PMA-ddPCR provides an accurate measure of DNA from viable cells, we next sought to determine whether PMA-ddPCR can accurately approximate the number of culturable bacteria. To this end, we used serial dilutions of a skin-resident bacterial species, *Staphylococcus epidermidis,* and generated a standard curve correlating DNA abundance (quantified by PMA-ddPCR) and CFU/mL (quantified by classical plating). We found that the PMA-ddPCR and CFU/mL values were highly correlated (Fig. S1B). Performing ddPCR without the use of PMA on an exponentially-growing population of *S. epidermidis* yielded similar results, indicating both that the PMA treatment itself does not significantly alter viability and that an exponentially-growing culture of bacteria is comprised of mostly viable cells (Fig. S1C). Together, these controls confirm that PMA-ddPCR represents a good proxy for the amount of DNA in a sample present within intact bacteria.

We next collected human skin microbiome samples using sterile swabbing technique to determine if our findings with *in vitro* bacterial cultures extend to skin microbiome samples. To quantify the number of viable bacteria directly, we plated a small amount of each sample using the standard conditions for culturing skin microbes (5% sheep blood in tryptic soy agarose plates incubated both aerobically and anaerobically). To determine whether PMA-ddPCR or traditional ddPCR better represented the number of viable skin microbiome bacteria, we split each sample into two equal halves and treated one half with PMA prior to DNA isolation, leaving the other half untreated. We quantified bacterial DNA in both samples by ddPCR using universal bacterial 16S primers. We found that for each sample, the PMA-ddPCR quantification closely matched the standard curve generated with *S. epidermidis,* suggesting that the use of PMA allows for an accurate quantification of viable bacterial DNA (Fig. 2 B). More specifically, quantifying the bacterial DNA in skin microbiome samples without the use of PMA resulted in DNA quantities that were, on average, 82 times higher than predicted by the standard curve, while the use of PMA brought this value down to just 1.3 (Fig. 2 C). Using ddPCR counts to predict CFU showed similar results, as ddPCR in the absence of PMA yielded values that predicted CFU counts 58.5 times greater than those measured, while PMA-ddPCR yielded values that predicted CFU counts that were on average only 1.28 times greater than the actual cultured CFU (Fig. 2 D).

Calculating the ratio of ddPCR counts between samples without PMA and samples with PMA allowed us to generate a viability score for any given microbiome sample. Additionally, we calculated a CFU-based viability score by comparing the CFU predicted by the ddPCR counts in a sample without the use of PMA to the actual CFU. Using either the ddPCR-based method or the CFU-based method resulted in similar viability scores and allowed us to gauge the overall fraction of viable bacteria in a population (Fig. 2 E).

We next evaluated viability scores (using the PMA-ddPCR-based method) of DNA sampled from different skin microbiome sites by swabbing the skin of four healthy human volunteers at eight sites (glabella, retroauricular crease, lower back, hair shaft, antecubital fossa, popliteal fossa, nares, and dorsal forearm) (Fig. 2 F, Fig. S2). PMA-ddPCR revealed that the viability scores for these sites ranged between 0.02 and 0.12 (0 represents a fully-nonviable population, 1.0 represents a fully-viable population), indicating that the majority of bacterial DNA found on the skin surface is not associated with viable cells (Fig. 2 G). To investigate whether this was a skin-specific phenomenon, we tested several non-skin microbiome sites (tongue, saliva, plaque, and feces). We found that in all non-skin microbiome sites, the viability score was significantly higher than for the skin, ranging from 0.4 (saliva) to 0.87 (feces) (Fig. 2 G). These results provide independent support for our imaging-based findings that the skin surface is populated by few viable bacterial cells, indicating that the surface of healthy non-sterilized human skin is sparsely colonized. While these data indicate that bacterial DNA on the skin surface is predominantly not associated with viable bacterial cells, we note that our results do not suggest that there are no viable cells on the skin surface. Rather, our data indicate that the majority of the bacterial on the skin surface is not in intact bacteria such that specifically assessing the DNA associated with intact cells using PMA provides a much more accurate estimation of the viable skin microbiome.

Like many microbiomes, the existing knowledge of the skin microbiome is heavily based upon bacterial 16S rRNA gene amplicon sequencing, which was developed to assess bacterial populations while avoiding biases introduced by culturing methods. However, our findings suggest that using 16S rRNA gene amplicon sequencing to study the skin microbiome is not entirely unbiased, as most of the DNA in these samples is from nonviable bacteria and traditional

16S rRNA gene amplicon sequencing does not differentiate between DNA originating from live or dead cells. The inability of 16S rRNA gene amplicon sequencing to differentiate between these two types of bacterial populations has been mentioned as a potential downfall of the method, but has not been addressed (*8*). To evaluate how accurately traditional 16S rRNA gene amplicon sequencing captures the living skin microbiome composition, we utilized PMA followed by 16S rRNA gene amplicon sequencing (PMA-seq) (*21*). By sequencing pairs of matched samples with PMA treatment (PMA-seq) and without PMA treatment (traditional sequencing), we were able to explore how closely the microbiome compositions obtained from traditional sequencing methods resembled the viable microbiome composition obtained by PMA-seq. These experiments established that at each skin site sampled, as compared to traditional sequencing, the PMA-treated samples were less rich (richness, *R*, is a measure of the number of identifiable bacterial taxa) and less diverse (diversity, *H*, is measured by the Shannon diversity index) (Fig 3 A, B). Furthermore, samples that had greater richness in traditional sequencing ($R_{trad}$) showed proportionally larger decreases in richness and Shannon diversity with PMA-seq ($R_{PMA}$ and $H_{PMA}$) (Fig. 3B-C). These results suggest that, although it appears by traditional sequencing that there is a wide range of richness values at different skin sites (1-30 different taxa), in reality the richness across the skin microbiome at different body sites is relatively similar and low (1-10 different taxa). Though we did identify a small number of samples where the richness increased upon PMA treatment, these increases were due mostly to minor components of the microbiome (Fig. 3C), and these samples still showed a decrease in Shannon diversity (Fig. 3B). Thus, though there appears to be a wide range of diversity in the skin microbiome by traditional sequencing, PMA-seq indicates that this is generally an

158 overestimation at any given skin site. In fact, our results suggest that the viable skin microbiome
159 tends to be dominated by a relatively small number of taxa at most sites.

160 The metrics of richness and diversity offer important information regarding how the
161 composition of the skin microbiome changes at different body sites between traditional
162 sequencing and PMA-seq. However, we also wanted to understand the changes in the relative
163 abundance of specific bacterial taxa. To quantify taxon-level PMA-dependent changes, we
164 developed a PMA-index ($I_{PMA}$) for each bacterial taxon, which is calculated as follows:
165 $I_{PMA}=\frac{A_{PMA}}{(A_{PMA})+(A_{trad})}$, where $A_{PMA}$ is the relative abundance by PMA-seq and $A_{trad}$ is the relative
166 abundance by traditional sequencing. A low PMA-index (below 0.5) indicates that the taxon in
167 question is overrepresented by traditional sequencing, while a high PMA index (above 0.5)
168 indicates that the taxon in question is underrepresented by traditional sequencing (Fig 4A).
169 Calculating PMA-indices revealed that the abundances of most bacterial taxa at any given body
170 site are overestimated by traditional sequencing, as most taxa had PMA-index values close to 0
171 (Fig. 4A).

172 The three most abundant family-level bacterial families (*Propionibacteriaceae*,
173 *Corynebacteriaceae*, and *Micrococcaceae*) made up 93% of total sequencing reads (96% of
174 PMA-seq reads and 91% of traditional sequencing reads) and demonstrated interesting family-
175 level PMA-index patterns. The family *Propionibacteriaceae* includes a major component of the
176 skin microbiome, *C. acnes*, which has been shown by traditional sequencing to comprise
177 upwards of 50% of the skin microbiome irrespective of site type (*8*). PMA-seq revealed that
178 traditional sequencing accurately represents *Propionibacteriaceae* abundance in sebaceous sites
179 (demonstrated by a PMA-index close to 0.5), but overrepresents *Propionibacteriaceae* in moist
180 and dry sites (PMA-indices of 0.2-0.3). Furthermore, *Propionibacteriaceae* dominated sebaceous

sites (accounting for >75% of all viable bacteria in most sebaceous samples), but did not dominate moist or dry sites (their viable abundance did not exceed 50% of all viable bacteria in any of those samples).

Bacteria in the family *Corynebacteriaceae* are also considered main constituents of the skin microbiome, but our results showed that traditional sequencing overestimates the abundance of *Corynebacteriaceae* at every skin site except for the nares. For example, traditional sequencing identified a high abundance of *Corynebacteriaceae* in the popliteal fossa, but PMA-seq showed that these reads were largely of inviable origin (Fig. 4B). Previous studies have demonstrated that *Corynebacteria* are readily cultured from nasal isolates, which supports our PMA-seq finding that viable members of this taxon are abundant in the nares but not at most other skin sites (*22*).

Interestingly, *Micrococcaceae* were overrepresented by traditional sequencing at every site except for the hair shaft. In the hair shaft, *Micrococcaceae* were abundant by PMA-seq but almost undetectable by traditional sequencing. As shown in Figure 4B, the increase in the relative proportion of viable *Micrococcaceae* detected by PMA-seq corresponds to a decrease in viable *Propionibacteriaceae*, suggesting that *Micrococcaceae* may not be detected by traditional sequencing because of the high abundance of DNA from inviable *Propionibacteriaceae.* These results suggest that most skin sites are colonized by a relatively small number of bacterial families and that different families distinctly colonize different skin sites.

Our sequencing did not show an abundance of *Staphylococcus*, which is often (*12*, *13*, *23*), but not always (*24*), detected in the skin microbiome. We thus evaluated the viability of this genus using PMA-ddPCR with *Staphylococcus*-specific primers (Fig. S3). By using lysostaphin prior to DNA isolation, we ensured that any *Staphylococcus* present would be sufficiently lysed.

Comparisons with universal bacterial 16S primers confirmed that the inclusion of lysostaphin did not significantly change the overall viability scores at the body sites tested (Fig. S3). Meanwhile, our *Staphylococcus*-specific analysis confirmed that like other bacteria, *Staphylococcus* are also largely inviable on the skin surface (Fig. S3). These results reinforce our conclusion that the bulk of the bacterial DNA on the skin surface is from nonviable bacteria.

Finally, we were curious if our findings were human-specific, or if they also translated to murine systems. We thus assessed the spatial distribution of bacterial cells in mouse skin tissue. Using the universal bacterial FISH probe with tissue from K14-H2B-GFP mice revealed the same bacterial distributions as seen in the human tissues: a high abundance of bacteria in hair follicles (enrichment score of 15.26) with relatively few bacteria on the skin surface (enrichment score of 0.21) (Fig. 5 A, D). Given that one main function of the densely-packed coat of hair found on mammals like mice is to protect the skin surface from the outside environment, we wondered whether the lack of bacteria on the skin surface was due to their dense fur. To test how fur impacts the presence of bacteria on the skin surface, we performed FISH staining on skin from nude mice (SKH1-Hrhr Elite) and found similar bacterial distributions (follicle-associated enrichment score of 10.79 compared to 1.13 for the skin surface) (Fig. 5 B, D).

Since we failed to detect many bacteria on the surface of any of the skin samples tested, we sought a positive control to confirm that our FISH staining can visualize bacteria on the skin surface if they are present. To this end, we applied *Escherichia coli* cells to dorsal mouse skin tissue after removing it from the animal. This tissue was then processed in the same way as the human and other mouse tissue. FISH staining revealed many bacteria on the surface of these samples, confirming that this technique can be used to reliably visualize bacteria on the skin surface (Fig. 5 C). As a negative control, we also confirmed that a probe encoding the reverse

complement of the EUB338 FISH probe (NONEUB338) did not significantly stain the skin surface or follicles (Fig. 5 C).

Because our imaging of mouse skin suggested some similarity to human skin, we next decided to assess the viability of bacteria in the mouse skin microbiome using PMA-ddPCR. As further evidence that our previous findings are not human-specific, the PMA-ddPCR-based viability score for mouse skin microbiome sites was similar to the average viability score for human skin sites (0.066 and 0.045 respectively) and was much lower than the viability score for the mouse or human fecal microbiome (0.98 and 0.66 respectively). (Fig. 5E). Our results indicate that, despite having distinct skin biology, both humans and mice have an abundance of bacterial DNA on the skin surface that is not associated with viable cells. This observation suggests that the factors leading to this are also not unique to either given species and suggests that the presence of viable bacteria on the skin surface is rare for both humans and mice, and may thus represent a general phenomenon.

Here we used both imaging and PMA-based methods to demonstrate that the skin surface is sparsely colonized by bacteria. This central finding holds true across skin from human biopsies, healthy swabbed volunteers, hairy mice, and nude mice. The skin microbiome has garnered a great deal of attention as a means for educating the immune system, combatting pathogens, and promoting wound healing, and multiple groups are pursuing skin probiotics (*25*). Our findings have significant implications for the mechanisms underlying these skin microbiome functions, as well as for the ability to manipulate skin microbiome composition. For example, our findings support previous work suggesting that the key function of immune education by the skin microbiome occurs within hair follicles (*4*). Meanwhile, our results may explain why stably colonizing the skin surface with exogenous bacteria has proved to be difficult and often requires

abrasion (*3*). Disruption of the stratum corneum (skin surface layers), which occurs during skin abrasion, may allow access to the deeper layers of tissue where the stable bacterial populations reside. Thus, targeting the bacteria within hair follicles may represent a better strategy for stably manipulating the skin microbiome or educating the immune system. While it has been known for some time that bacteria inhabit hair follicles (*4*, *16*), our findings extend this knowledge and suggest that the viable bacteria of the skin microbiome are primarily restricted to these sites. This is further supported by our finding that bacteria can be readily cultured from the skin surface, but at far less abundance than suggested by the amount of bacterial DNA present on the skin.

Our results also offer some insight into the apparent paradox of skin microbiome stability, in which skin microbiome composition has been found to be extremely stable over long time scales but highly susceptible to transient perturbations. A longitudinal study found that individual skin microbiome composition is consistent across months, while another study found that ocean swimming dramatically altered skin microbiome composition within hours (*11*, *26*). The skin is primarily colonized by viable bacteria in pilosebaceous units and other skin invaginations and the bacterial DNA on the skin surface is mostly from dead bacteria. Thus, surface bacterial DNA could be easily washed away and replaced by other bacterial DNA from the environment, leading to low stability on short timescales. Meanwhile, the viable bacteria in hair follicles and other cutaneous structures may remain unperturbed by washing, persisting as a small but stable source of new bacterial DNA that replenishes the skin surface over time and leads to high stability at long timescales. In this scenario, hair follicles and other cutaneous structures could serve as the primary site of replication for the bacteria of the skin microbiome, which are eventually pushed out towards the skin surface. At the surface, the DNA from dead bacteria that originated from distinct skin sites can mix, which would provide an explanation for

why traditional sequencing overrepresents bacterial diversity. This model would also explain the counter-intuitive abundance of obligately anaerobic bacterial species associated with the skin microbiome. We note that human skin cells are also born in stem-cell-rich invaginations and are pushed to the surface as they die. In this way, the life cycle of the skin microbiome may resemble the process of epithelial cell turnover in the skin.

Our findings also raise fundamental questions that will need to be addressed by future studies focused on why the skin surface is poorly colonized. The accessible DNA in non-skin microbiomes is generally representative of viable bacterial cells, as all non-skin microbiomes tested had viability scores above 0.4. This is in stark contrast to the skin microbiome, which had viability scores between 0.02 and 0.12. Even saliva, which contains a multitude of antimicrobial compounds such as lysozyme, lactoferrin, lactoperoxidase, and antimicrobial peptides (*27*), had a viability score nearly four times greater than the highest viability score for a skin microbiome. The uniquely low viability score associated with the skin could be explained by passive mechanisms, like bacterial DNA adhering to the skin long after a bacterial cell dies. Alternatively, there could be active mechanisms like bacterial killing on the skin surface by factors like antimicrobial peptides produced by epithelial cells, competition between bacterial species, or exposure to harsh environmental factors such as starvation, UV radiation, or desiccation.

In conclusion, we have shown for the first time the spatial distribution of the viable skin microbiome in its native state. Our data challenge the assumption that the skin surface is replete with viable bacterial cells, and suggest instead that the bacterial DNA on the skin surface is not representative of the viable bacterial population. Our findings also suggest that traditional 16S rRNA gene amplicon sequencing is not sufficient for analyzing bacterial communities like the

skin microbiome, as it leads to overestimation of richness and diversity and can lead to inaccurate assessment of bacterial abundance. PMA-seq is thus a powerful tool for assessing the viable components of a complex community, and, when coupled with traditional sequencing, can also evaluate how closely the available DNA reflects the viable components within a community. Our results provide an essential step towards a complete understanding of the functional skin microbiome and suggest a more accurate method to evaluate bacterial communities on the skin surface.

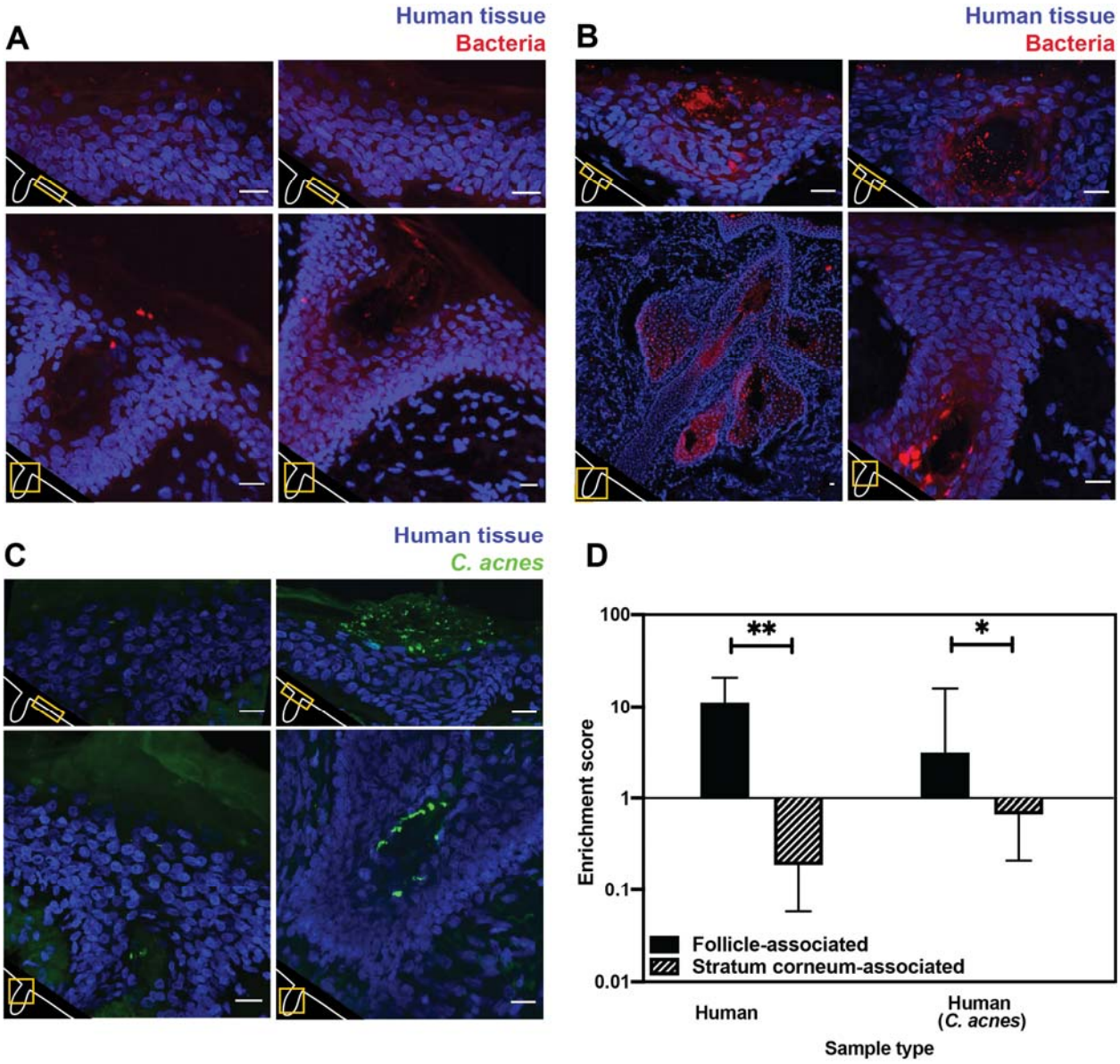


304

305 **Fig. 1.** Bacterial FISH staining of human tissue. (A-C) Scale bar = 20 µm. The bottom left corner
306 of each diagram shows a schematic of the hair follicle in white and the anatomic location of each
307 image frame in yellow. DAPI staining is shown in blue in all parts. EUB338 hybridization is
308 shown in red for all images. (A) Human tissues stained with the pan-bacterial FISH probe
309 EUB338 show little bacterial presence at the skin surface. (B) Human tissues stained with
310 EUB338 show abundant bacterial signal that is concentrated in hair follicles, pilosebaceous units,

311 and other cutaneous structures. (C) Human tissues stained with a *C. acnes* specific FISH probe
312 (in green) demonstrate the same overall spatial organization as those stained with EUB338. (D)
313 Quantification enrichment scores showing the median and interquartile range. Significance was
314 calculated using the Mann-Whitney test. *$P \leq 0.05$, **$P \leq 0.01$. N = 8 for human follicle, N = 6
315 for human follicle (*C. acnes*) and human stratum corneum, N = 5 for human stratum corneum (*C.*
316 *acnes*).
317

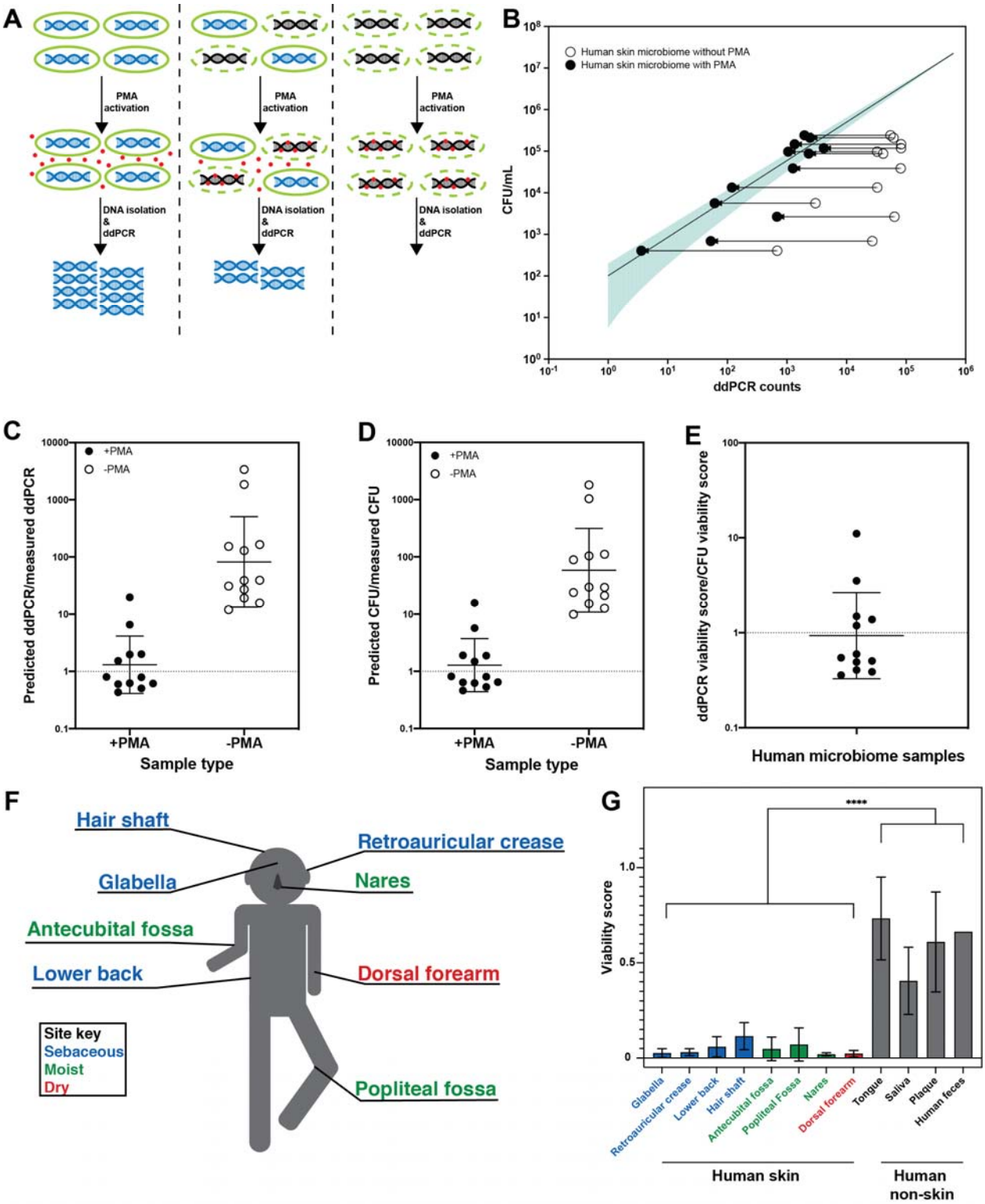


**Fig. 2.** PMA-ddPCR and viability scores for human skin and non-skin microbiomes . (A) Schematic of the PMA-ddPCR workflow. (B) Standard curve generated using *Staphylococcus*

*epidermidis* cultures shown in green. Shading represents 95% confidence interval. Open and closed circles represent skin microbiome samples that did (closed circles) or did not (open circles) receive PMA treatment. Paired samples are connected with a left-facing arrow to show the downward shift in DNA abundance with the inclusion of PMA. (C) Comparison of the predicted ddPCR counts to measured ddPCR counts based on CFU for samples that were treated with PMA (closed circles) and samples that were not treated with PMA (open circles) (mean for PMA-treated samples is 1.31, mean for untreated samples is 82.2) . (D) Comparison of the predicted CFU to measured CFU based on ddPCR for samples that were treated with PMA (closed circles) and samples that were not treated with PMA (open circles) (mean for PMA treated samples is 1.28, mean for untreated samples is 58.5). (E) Comparison of ddPCR-based viability score to CFU-based viability score (mean = 0.93). (F) Sampling scheme showing each skin site that was sampled. Colors indicate site-type (sebaceous in blue, moist in green, dry in red). (G) PMA-ddPCR on skin and non-skin microbiome sites shows that the viability score of the skin microbiome is significantly lower than other microbiome sites. ****$P \leq 0.0001$ for Student's T Test on pooled skin and non-skin samples. Four volunteers contributed skin and non-skin microbiome samples. Additional samples were collected from some individuals and represent biological replicates. N= 8 for glabella, N = 6 for retroarticular crease, N = 5 for lower back, hair shaft, nares, and dorsal forearm, N = 3 for antecubital fossa, tongue, saliva, and plaque, N = 2 for popliteal fossa, and N = 1 for human feces. For raw ddPCR counts, see Fig. S2.

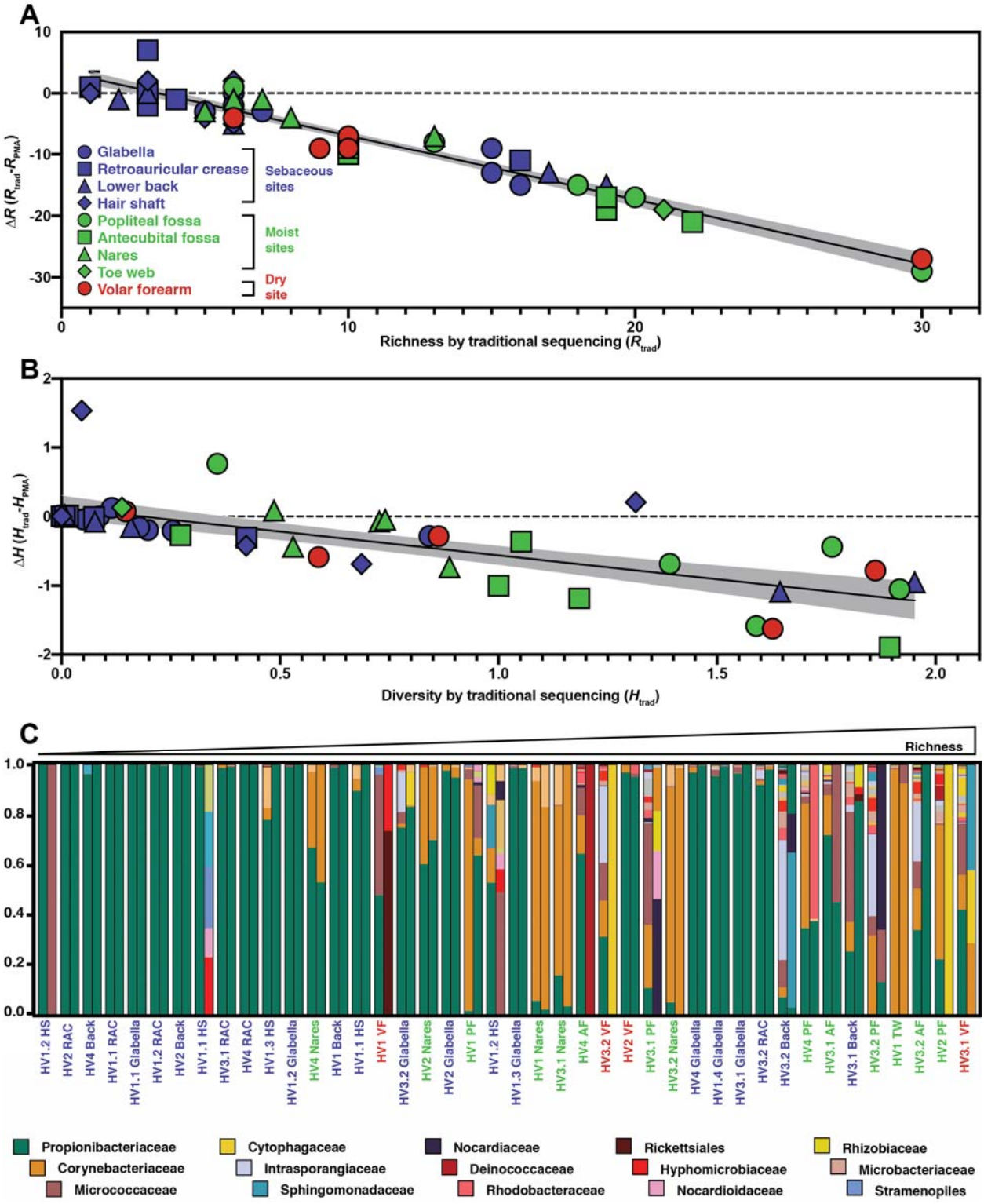


**Fig. 3.** Richness and Shannon diversity of traditional sequencing compared to PMA-seq. (A) The richness changes between traditional sequencing ($R_{trad}$) and PMA-seq ($R_{PMA}$) are demonstrated

by plotting the change in richness ($\Delta R$) against $R_{trad}$. Colors represent different site types and shapes represent different sample sites. The shaded gray region represents the 95% confidence interval for the linear regression. (B) The Shannon diversity changes between traditional sequencing ($H_{trad}$) and PMA-seq ($H_{PMA}$) are demonstrated by plotting the change in diversity ($\Delta H$) against $H_{trad}$. Colors, shapes, and gray shading are the same as in (A). (C) Relative abundance of the 15 most abundant bacterial taxa overall (listed in descending order below). Paired bars represent data from traditional sequencing (left) and PMA-seq (right). Samples are ordered by increasing richness in traditional sequencing. Labels below each pair of bars indicate each sample's donor, replicate, and site (for example, HV1.1 RAC indicates Healthy Volunteer 1, replicate sample 1, retroauricular crease). HS: hair shaft, RAC: retroauricular crease, VF: volar forearm, PF: popliteal fossa, TW: toe web, AF: antecubital fossa.

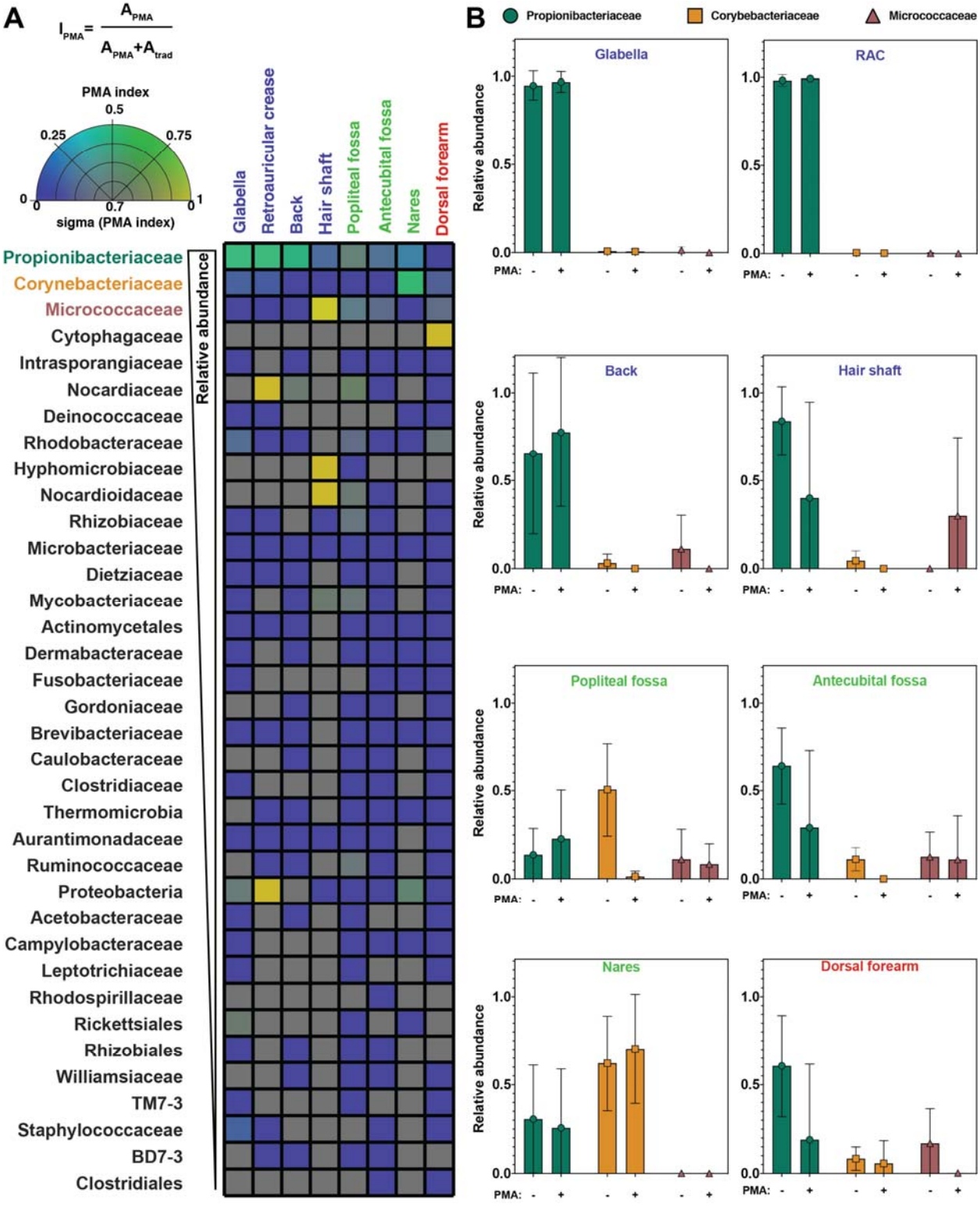


**Fig. 4.** PMA index. (A) The PMA index for each bacterial taxon that was present in at least 4 samples is shown here as an average between samples of the same sample site. Color indicates

PMA index value. Saturation indicates confidence (sigma) in the PMA index value and was calculated using the standard deviation of PMA index across the samples that went into that pixel. Bacterial taxa are ordered by decreasing overall relative abundance. Each square represents the average of at least four samples taken from different individuals. PMA-index is calculated by comparing the relative abundance of a given taxon as measured by PMA-seq ($A_{PMA}$) to the sum of the relative abundance for that taxon in both traditional sequencing ($A_{trad}$) and PMA-seq. (B) Relative abundance at each body site for the top three most abundant (overall) bacterial taxa as assessed by traditional sequencing and PMA-seq. Colors of bars correspond to colors in Figure 2F.

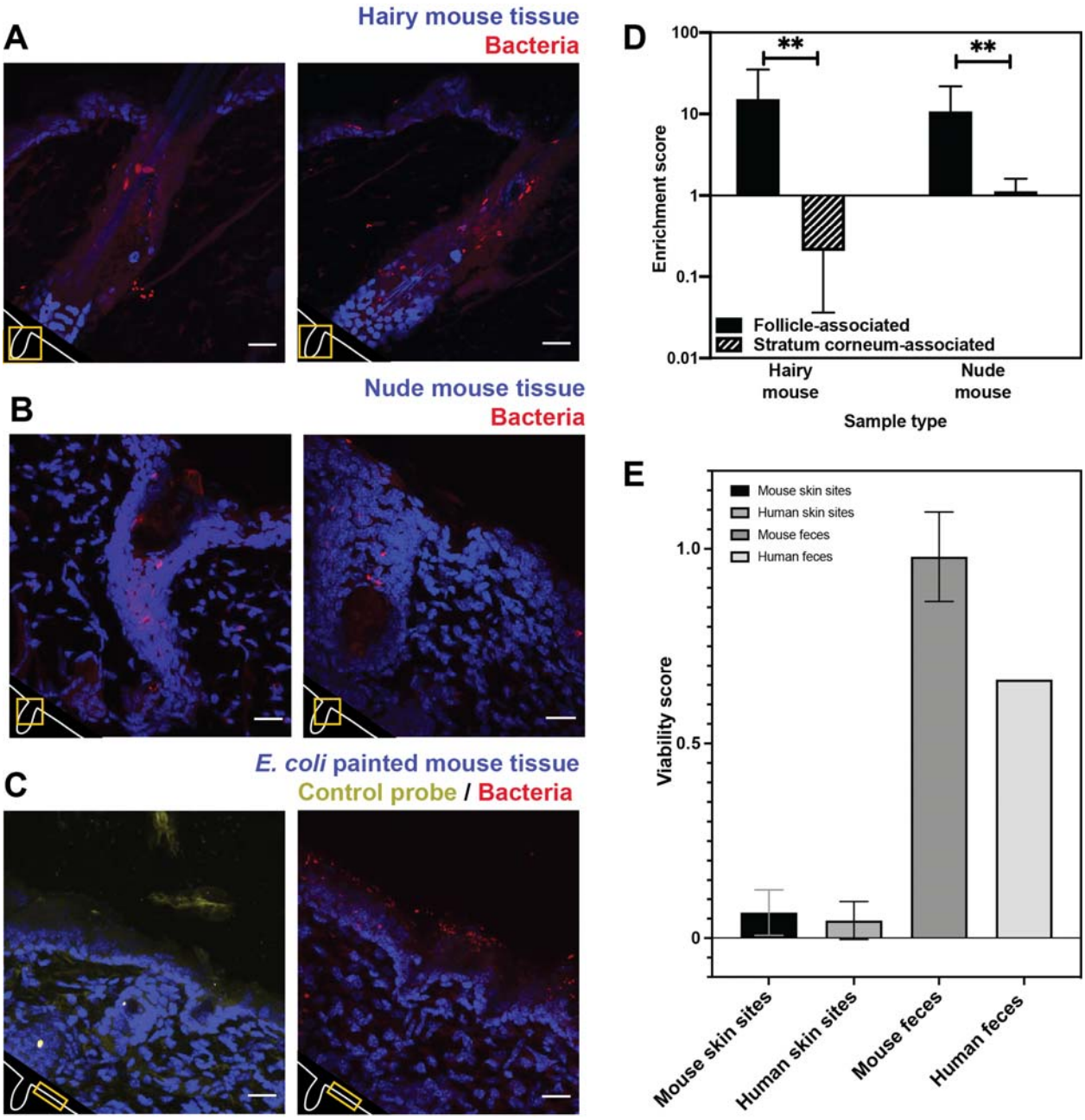


**Fig 5.** Bacterial FISH staining of mouse tissue (A-D) and comparison of mouse viability scores and human viability scores. (A). Tissues from a K14-H2B_GFP mouse stained with EUB338 show abundant bacterial signal in hair follicles but not on the skin surface. (B) Tissues from SKH1-Hrhr Elite nude mice also show bacterial presence concentrated to cutaneous structures and not at the skin surface. (C) E. coli applied to C57BL/6 mouse tissue was stained with either EUB338 (in red) or its complementary strand control probe NONEUB338 (in yellow). (D)

377 Quantification enrichment scores showing the median and interquartile range. Significance was
378 calculated using the Mann-Whitney test. *P ≤ 0.05, **P ≤ 0.01, N = 6 for hairy mouse follicle,
379 nude mouse follicle, and hairy mouse stratum corneum, N = 5 nude mouse stratum corneum. (E)
380 The PMA-ddPCR-based viability scores for mouse skin microbiomes are much lower than for
381 mouse fecal microbiomes (0.66 and 0.98 respectively). These viability scores for mouse sites are
382 very similar to those for humans (0.66 and 0.45 for skin microbiomes, 0.98 and 0.66 for fecal
383 microbiomes).
384

## Materials and Methods

### Human and mouse tissue processing

Human tissue was obtained through the Skin Translational Research Core within the Skin Biology and Diseases Resource-based Center (SBDRC) at the University of Pennsylvania. Samples were obtained from healthy tissue in patients undergoing skin surgical procedures. Samples were embedded in OCT and stored at -80ºC prior to sectioning.

All mice were housed and maintained in a certified animal facility and all experiments were conducted according to USA Public Health Service Policy of Humane Care and Use of Laboratory Animals. All protocols were approved by the Institutional Animal Care and Use Committee, protocol #1867-17 (Princeton University). Dorsal skin from K14-H2B-GFP, C57BL/6, and SKH1-Elite nude mice was used for fluorescence experiments. The fur from K14-H2B-GFP and C57BL/6 mice was shaved using clippers prior to embedding in OCT. Both sexes were used.

### Fluorescence in situ hybridization and imaging

Human and mouse tissues were processed identically. 30 µm tissue sections were sectioned and mounted on slides using a Leica CM3050S cryostat. Tissues on slides were fixed in 4% formaldehyde in 1X PBS for 20 mins. Following fixation, tissues were washed for 5 mins in 1X PBS and then incubated in hybridization buffer (0.9 M NaCl, 20 mM Tris-HCl, 10% formamide) containing 10 mg/mL lysozyme and FISH probes at 1 µg/µL for 2-3 hours at 47ºC in the dark. Nucleotide sequences of FISH probes can be found in Table S1. After hybridization, slides were incubated in wash buffer (0.9 M NaCl, 20 mM Tris-HCl) for 1 hr at 47ºC in the dark. Slides were then washed in 1X PBS for 10 mins. To visualize tissue nuclei, tissues were then

stained with 1 µg/mL DAPI for 10 mins at room temperature. Slides were then washed 3X in 1X PBS for 10 mins each. Following the final wash step, tissues were mounted with glycerol-based anti-fade non-curing mounting media. Coverslips were sealed using a 1:1:1 mixture of petroleum jelly, lanolin, and paraffin. Images were acquired on a Nikon A1R-Si HD confocal microscope controlled by NIS Elements software. ImageJ and MATLAB (Mathworks, Natwick, MA) were used for image processing. To calculate fluorescence enrichment scores, maximum projections of Z-stacks were used. A rectangular region of interest (ROI) of width W was drawn around a follicle using only the DAPI channel. A second ROI was drawn near the follicle opening with dimensions 0.5W x 2W in order to capture follicle-associated fluorescence near the follicle opening. In an orthogonal processing step, the pixel intensities for the entire image in the FISH fluorescent channel were fit using a 3 component Gaussian mixture model (GMM) corresponding roughly to non-tissue background, non-probe autofluorescence, and probe-based signal. Using this GMM as the background subtraction value for each image, the mean intensity for each ROI was calculated. This threshold value was used to calculate the mean fluorescence value inside the ROI and outside the ROI. The ratio of the mean fluorescence value inside the ROI to the mean fluorescence value outside of the ROI was used for quantifying follicle- and stratum corneum-associated fluorescence (enrichment score). Significance was calculated using the Mann-Whitney test.

**Human subject microbiome samples**

Microbiome samples were collected under Princeton University IRB #13003 at the Princeton University Department of Molecular Biology. Participants were healthy volunteers,

aged 26-35, with no history of chronic skin conditions or autoimmune disease and were not using antibiotics.

Skin microbiomes from healthy volunteers were collected using sterile foam-tipped collection swabs pre-moistened with sterile 1X DPBS. Though often included, we chose not to use detergent in the swabbing buffer in order to avoid negatively affecting bacterial cell membranes and altering viability scores. Fig. S1D shows how swabbing with and without 0.1% Triton X-100 (Sigma) affects viability scores, ddPCR results, and CFU. Areas of interest were sampled for 60 seconds before being re-suspended in sterile 1X DPBS. Tongue microbiome samples were collected using sterile foam-tipped collection swabs. Hair shaft samples were collected by plucking hairs and using only the bulb portion. Saliva was collected in sterile 50 mL conicals from healthy volunteers. Plaque was collected by scraping the teeth of healthy volunteers using sterile toothpicks and re-suspending the collection in sterile 1X DPBS. Murine fecal samples from C57BL/6 mice were collected during dissection. Human skin microbiome samples shown in Figure 2B-E were plated for CFU calculations prior to the addition of PMA. Samples were plated on blood agar plates (5% sheep blood in tryptic soy agar, VWR International) and grown for 24-48 hours aerobically or anaerobically.

The human fecal sample was collected by the Donia lab under Princeton University IRB #11606 and was gifted to the Gitai lab.

**Heat-killed *E. coli* ratios**

In order to demonstrate the efficacy of PMA, known ratios of live and heat-killed *E. coli* cultures were mixed and subjected to PMA treatment. First, an overnight culture of *E. coli* NCM3722 was back-diluted into fresh LB media at a ratio of 1:1000 and grown at 37°C for 4 hours to reach

mid-log. Half of the exponentially-growing culture was heat-killed by incubating at 70°C for 20 minutes while the other half remained at room temperature. The heat-killed *E. coli* cultures were allowed to cool to room temperature before combining with non-heat-killed *E. coli* cultures to achieve a 50% (by volume) heat-killed mixture. For the 0% heat-killed, no heat-killed bacteria were added. Likewise, for the 100% heat-killed, only heat-killed bacteria were used. Each condition was mixed well and then split evenly between two sterile 1.5 mL microcentrifuge tubes.

**Propidium monoazide (PMA) treatment and DNA isolation**

After collection, samples were split evenly between two sterile 1.5 mL microcentrifuge tubes. PMA (Biotium Inc.) was added to one of the two tubes to a final concentration of 50 µM. All tubes were incubated in the dark at room temperature for 10 mins before being exposed to light to cross-link PMA molecules using the PMA-Lite™ LED Photolysis Device (Biotium Inc.). DNA was then isolated from all samples using the DNeasy PowerSoil Kit (Qiagen). If lysostaphin (Sigma-Aldrich) was used, it was added following PMA activation and before DNA isolation to a final concentration of 0.1 mg/mL and incubated at room temperature for 30 mins.

**Droplet digital PCR (ddPCR)**

The Bio Rad QX200 AutoDG Droplet Digital PCR System was used to quantify extracted DNA from microbiome samples and from pure bacterial cultures. Reaction mixtures contained 2x QX200 ddPCR EvaGreen Supermix and universal 16S qPCR primers at 10 nM concentrations in a total volume of 25 µL. Primer sequences can be found in Table S1. Reaction mixtures were transferred to sterile ddPCR 96-well plates (BioRad #12001925) which were

loaded into the QX200 Automated Droplet Generator. After droplet generation, the plate was heat-sealed using the PX1 PCR Plate Sealer (BioRad #1814000) and PCR was performed with a pre-step of 95 C for 5 minutes followed by 40 rounds of amplification with 60C, 1 minute extensions and a final hold temperature of 12 C using a C1000 Touch Thermal Cycler (BioRad #1851197). Samples were subsequently loaded into the QX200 Droplet Reader for quantification. Automatic thresholding was performed using the Quantasoft software and subsequently exported to Microsoft Excel for analysis. Significance was calculated using a Student's T-Test. To calculate the viability score for a given pair of "-PMA" and "+PMA" matched samples, the following calculation was done:

$$\frac{Copies\ per\ 20\ \mu L\ without\ PMA}{Copies\ per\ 20\ \mu L\ with\ PMA}$$

**_Staphylococcus epidermidis_ ddPCR and CFU standard curve**

Cultures of *S. epidermidis* EGM 2-06 were grown in tryptic soy broth (TSB) overnight and diluted 1:1000 the following morning in TSB and grown for 4 hours until a final OD of 0.4. Tenfold dilutions of *S. epidermidis* culture were then prepared, plated for CFU on 5% sheep blood in tryptic soy agar (VWR International) and divided between two 1.5 mL microcentrifuge tubes. PMA was added to one tube for a final concentration of 50 µM and the other tube was left untreated. PMA activation and DNA isolation was then done according to the methods outlined above.

**16S rRNA gene amplicon sequencing**

DNA was isolated from microbiome samples (with and without PMA) using the DNeasy PowerSoil Kit (Qiagen). The V1-V3 region of the 16S gene was amplified using the primers 27F (5'- AGAGTTTGATCCTGGCTCAG) and 534R (5'- ATTACCGCGGCTGCTGG). Illumina sequencing libraries were prepared using previously published primers (*28*). Libraries were then pooled at equimolar ratios and sequenced on an Illumina MiSeq Micro 500 nt as paired-end reads. Reads were 2X250 bp with an average depth of ~33,616 reads. Also included were 8 bp Index reads, following the manufacturer's protocol (Illumina, USA). Raw sequencing reads were filtered by Illumina HiSeq Control Software to generate Pass-Filter reads for further analysis. Index reads were used for sample de-multiplexing. Amplicon sequencing variants (ASVs) were then inferred from the unmerged paired-end sequences using the DADA2 plugin within QIIME2 version 2018.6 (*29*, *30*). Reads were not trimmed. Taxonomy was assigned to the resulting ASVs with a naive Bayes classifier trained on the Greengenes database version using only the target region of the 16S rRNA gene. 13.8 (*31*, *32*). All downstream analyses were performed using family-level taxonomy assignments. Sequencing counts that were present in blank controls were subtracted. Relative abundance, richness, Shannon diversity, and PMA-index were assessed using the Vegan package for R or Microsoft Excel and plotted using R, Prism, and MATLAB (*33*). The PMA-index was calculated using relative abundance and was not calculated for any bacterial taxa that was present in fewer than four samples.

**Data availability**

The datasets generated during and/or analyzed during the current study are available from the corresponding author on reasonable request.

## References

1. R. L. Gallo, Human Skin Is the Largest Epithelial Surface for Interaction with Microbes. *J. Invest. Dermatol.* **137** (2017), pp. 1213–1214.

2. K. Maeda, New method of measurement of epidermal turnover in humans. *Cosmetics* (2017), doi:10.3390/cosmetics4040047.

3. T. C. Scharschmidt, K. S. Vasquez, H. A. Truong, S. V. Gearty, M. L. Pauli, A. Nosbaum, I. K. Gratz, M. Otto, J. J. Moon, J. Liese, A. K. Abbas, M. A. Fischbach, M. D. Rosenblum, A Wave of Regulatory T Cells into Neonatal Skin Mediates Tolerance to Commensal Microbes. *Immunity*. **43**, 1011–1021 (2015).

4. K. Polak-Witka, L. Rudnicka, U. Blume-Peytavi, A. Vogt, The role of the microbiome in scalp hair follicle biology and disease. *Exp. Dermatol.* (2020), , doi:10.1111/exd.13935.

5. L. R. Kalan, J. S. Meisel, M. A. Loesche, J. Horwinski, I. Soaita, X. Chen, A. Uberoi, S. E. Gardner, E. A. Grice, Strain- and Species-Level Variation in the Microbiome of Diabetic Wounds Is Associated with Clinical Outcomes and Therapeutic Efficacy. *Cell Host Microbe* (2019), doi:10.1016/j.chom.2019.03.006.

6. J. H. Kim, B. Yang, A. Tedesco, E. G. D. Lebig, P. M. Ruegger, K. Xu, J. Borneman, M. Martins-Green, High Levels of Oxidative Stress and Skin Microbiome are Critical for Initiation and Development of Chronic Wounds in Diabetic Mice. *Sci. Rep.* **9**, 1–16 (2019).

7. M. Loesche, S. E. Gardner, L. Kalan, J. Horwinski, Q. Zheng, B. P. Hodkinson, A. S. Tyldsley, C. L. Franciscus, S. L. Hillis, S. Mehta, D. J. Margolis, E. A. Grice, Temporal Stability in Chronic Wound Microbiota Is Associated With Poor Healing. *J. Invest. Dermatol.* **137**, 237–244 (2017).

8. A. L. Byrd, Y. Belkaid, J. A. Segre, The human skin microbiome. *Nat. Rev. Microbiol.* (2018), , doi:10.1038/nrmicro.2017.157.

9. J. S. Meisel, G. Sfyroera, C. Bartow-McKenney, C. Gimblet, J. Bugayev, J. Horwinski, B. Kim, J. R. Brestoff, A. S. Tyldsley, Q. Zheng, B. P. Hodkinson, D. Artis, E. A. Grice, Commensal microbiota modulate gene expression in the skin. *Microbiome* (2018), doi:10.1186/s40168-018-0404-9.

10. T. C. Scharschmidt, K. S. Vasquez, M. L. Pauli, E. G. Leitner, K. Chu, H. A. Truong, M. M. Lowe, R. Sanchez Rodriguez, N. Ali, Z. G. Laszik, J. L. Sonnenburg, S. E. Millar, M. D. Rosenblum, Commensal Microbes and Hair Follicle Morphogenesis Coordinately Drive Treg Migration into Neonatal Skin. *Cell Host Microbe* (2017), doi:10.1016/j.chom.2017.03.001.

11. M. C. Nielsen, S. C. Jiang, Alterations of the human skin microbiome after ocean water exposure. *Mar. Pollut. Bull.* (2019), doi:10.1016/j.marpolbul.2019.06.047.

12. A. L. Byrd, Y. Belkaid, J. A. Segre, The human skin microbiome. *Nat. Rev. Microbiol.* **16** (2018), pp. 143–155.

13. E. A. Grice, J. A. Segre, The skin microbiome. *Nat. Rev. Microbiol.* (2011), , doi:10.1038/nrmicro2537.

14. C. Huttenhower, D. Gevers, R. Knight, S. Abubucker, J. H. Badger, A. T. Chinwalla, H. H. Creasy, A. M. Earl, M. G. Fitzgerald, R. S. Fulton, M. G. Giglio, K. Hallsworth-Pepin, E. A. Lobos, R. Madupu, V. Magrini, J. C. Martin, M. Mitreva, D. M. Muzny, E. J. Sodergren, J. Versalovic, A. M. Wollam, K. C. Worley, J. R. Wortman, S. K. Young, Q. Zeng, K. M. Aagaard, O. O. Abolude, E. Allen-Vercoe, E. J. Alm, L. Alvarado, G. L. Andersen, S. Anderson, E. Appelbaum, H. M. Arachchi, G. Armitage, C. A. Arze, T.

566 Ayvaz, C. C. Baker, L. Begg, T. Belachew, V. Bhonagiri, M. Bihan, M. J. Blaser, T.
567 Bloom, V. Bonazzi, J. Paul Brooks, G. A. Buck, C. J. Buhay, D. A. Busam, J. L.
568 Campbell, S. R. Canon, B. L. Cantarel, P. S. G. Chain, I. M. A. Chen, L. Chen, S.
569 Chhibba, K. Chu, D. M. Ciulla, J. C. Clemente, S. W. Clifton, S. Conlan, J. Crabtree, M.
570 A. Cutting, N. J. Davidovics, C. C. Davis, T. Z. Desantis, C. Deal, K. D. Delehaunty, F. E.
571 Dewhirst, E. Deych, Y. Ding, D. J. Dooling, S. P. Dugan, W. Michael Dunne, A. Scott
572 Durkin, R. C. Edgar, R. L. Erlich, C. N. Farmer, R. M. Farrell, K. Faust, M. Feldgarden,
573 V. M. Felix, S. Fisher, A. A. Fodor, L. J. Forney, L. Foster, V. Di Francesco, J. Friedman,
574 D. C. Friedrich, C. C. Fronick, L. L. Fulton, H. Gao, N. Garcia, G. Giannoukos, C. Giblin,
575 M. Y. Giovanni, J. M. Goldberg, J. Goll, A. Gonzalez, A. Griggs, S. Gujja, S. Kinder
576 Haake, B. J. Haas, H. A. Hamilton, E. L. Harris, T. A. Hepburn, B. Herter, D. E.
577 Hoffmann, M. E. Holder, C. Howarth, K. H. Huang, S. M. Huse, J. Izard, J. K. Jansson, H.
578 Jiang, C. Jordan, V. Joshi, J. A. Katancik, W. A. Keitel, S. T. Kelley, C. Kells, N. B. King,
579 D. Knights, H. H. Kong, O. Koren, S. Koren, K. C. Kota, C. L. Kovar, N. C. Kyrpides, P.
580 S. La Rosa, S. L. Lee, K. P. Lemon, N. Lennon, C. M. Lewis, L. Lewis, R. E. Ley, K. Li,
581 K. Liolios, B. Liu, Y. Liu, C. C. Lo, C. A. Lozupone, R. Dwayne Lunsford, T. Madden, A.
582 A. Mahurkar, P. J. Mannon, E. R. Mardis, V. M. Markowitz, K. Mavromatis, J. M.
583 McCorrison, D. McDonald, J. McEwen, A. L. McGuire, P. McInnes, T. Mehta, K. A.
584 Mihindukulasuriya, J. R. Miller, P. J. Minx, I. Newsham, C. Nusbaum, M. Oglaughlin, J.
585 Orvis, I. Pagani, K. Palaniappan, S. M. Patel, M. Pearson, J. Peterson, M. Podar, C. Pohl,
586 K. S. Pollard, M. Pop, M. E. Priest, L. M. Proctor, X. Qin, J. Raes, J. Ravel, J. G. Reid, M.
587 Rho, R. Rhodes, K. P. Riehle, M. C. Rivera, B. Rodriguez-Mueller, Y. H. Rogers, M. C.
588 Ross, C. Russ, R. K. Sanka, P. Sankar, J. Fah Sathirapongsasuti, J. A. Schloss, P. D.

Schloss, T. M. Schmidt, M. Scholz, L. Schriml, A. M. Schubert, N. Segata, J. A. Segre, W. D. Shannon, R. R. Sharp, T. J. Sharpton, N. Shenoy, N. U. Sheth, G. A. Simone, I. Singh, C. S. Smillie, J. D. Sobel, D. D. Sommer, P. Spicer, G. G. Sutton, S. M. Sykes, D. G. Tabbaa, M. Thiagarajan, C. M. Tomlinson, M. Torralba, T. J. Treangen, R. M. Truty, T. A. Vishnivetskaya, J. Walker, L. Wang, Z. Wang, D. V. Ward, W. Warren, M. A. Watson, C. Wellington, K. A. Wetterstrand, J. R. White, K. Wilczek-Boney, Y. Wu, K. M. Wylie, T. Wylie, C. Yandava, L. Ye, Y. Ye, S. Yooseph, B. P. Youmans, L. Zhang, Y. Zhou, Y. Zhu, L. Zoloth, J. D. Zucker, B. W. Birren, R. A. Gibbs, S. K. Highlander, B. A. Methé, K. E. Nelson, J. F. Petrosino, G. M. Weinstock, R. K. Wilson, O. White, Structure, function and diversity of the healthy human microbiome. *Nature* (2012), doi:10.1038/nature11234.

15. Y. Belkaid, S. Tamoutounour, The influence of skin microorganisms on cutaneous immunity. *Nat. Rev. Immunol.* (2016), , doi:10.1038/nri.2016.48.

16. M. B. Lousada, T. Lachnit, J. Edelkamp, T. Rouillé, D. Ajdic, Y. Uchida, A. Di Nardo, T. C. G. Bosch, R. Paus, Exploring the human hair follicle microbiome*. *Br. J. Dermatol.* (2021), , doi:10.1111/bjd.19461.

17. R. I. Amann, B. J. Binder, R. J. Olson, S. W. Chisholm, R. Devereux, D. A. Stahl', "Combination of 16S rRNA-Targeted Oligonucleotide Probes with Flow Cytometry for Analyzing Mixed Microbial Populations" (1990).

18. R. D. Bjerre, L. W. Hugerth, F. Boulund, M. Seifert, J. D. Johansen, L. Engstrand, Effects of sampling strategy and DNA extraction on human skin microbiome investigations. *Sci. Rep.* **9**, 1–11 (2019).

19. A. Nocker, C. Y. Cheung, A. K. Camper, Comparison of propidium monoazide with

ethidium monoazide for differentiation of live vs. dead bacteria by selective removal of DNA from dead cells. *J. Microbiol. Methods.* **67**, 310–320 (2006).

20. Y. Yang, D. Cheng, Y. Li, L. Yu, K. Y. H. Gin, J. P. Chen, M. Reinhard, Effects of monochloramine and hydrogen peroxide on the bacterial community shifts in biologically treated wastewater. *Chemosphere* (2017), doi:10.1016/j.chemosphere.2017.09.087.

21. A. Nocker, T. Richter-Heitmann, R. Montijn, F. Schuren, R. Kort, Discrimination between live and dead cells in bacterial communities from environmental water samples analyzed by 454 pyrosequencing. *Int. Microbiol.* (2010), doi:10.2436/20.1501.01.111.

22. Q. Liu, Q. Liu, H. Meng, H. Lv, Y. Liu, J. Liu, H. Wang, L. He, J. Qin, Y. Wang, Y. Dai, M. Otto, M. Li, Staphylococcus epidermidis Contributes to Healthy Maturation of the Nasal Microbiome by Stimulating Antimicrobial Peptide Production. *Cell Host Microbe*. **27**, 68-78.e5 (2020).

23. E. A. Grice, H. H. Kong, S. Conlan, C. B. Deming, J. Davis, A. C. Young, N. C. S. NISC Comparative Sequencing Program, G. G. Bouffard, R. W. Blakesley, P. R. Murray, E. D. Green, M. L. Turner, J. A. Segre, Topographical and temporal diversity of the human skin microbiome. *Science* (2009), doi:10.1126/science.1171700.

24. S. Huang, N. Haiminen, A.-P. Carrieri, R. Hu, L. Jiang, L. Parida, B. Russell, C. Allaband, A. Zarrinpar, Y. Vázquez-Baeza, P. Belda-Ferre, H. Zhou, H.-C. Kim, A. D. Swafford, R. Knight, Z. Z. Xu, Human Skin, Oral, and Gut Microbiomes Predict Chronological Age. *mSystems* (2020), doi:10.1128/msystems.00630-19.

25. Y. Yu, S. Dunaway, J. Champer, J. Kim, A. Alikhan, Changing our microbiome: probiotics in dermatology. *Br. J. Dermatol.* (2020), , doi:10.1111/bjd.18088.

26. J. Oh, A. L. Byrd, M. Park, H. H. Kong, J. A. Segre, Temporal Stability of the Human

635 Skin Microbiome. *Cell* (2016), doi:10.1016/j.cell.2016.04.008.

636 27. W. Van'T Hof, E. C. I. Veerman, A. V. N. Amerongen, A. J. M. Ligtenberg,

637 Antimicrobial defense systems in saliva. *Monogr. Oral Sci.* (2014),

638 doi:10.1159/000358783.

639 28. J. G. Caporaso, C. L. Lauber, W. A. Walters, D. Berg-Lyons, J. Huntley, N. Fierer, S. M.

640 Owens, J. Betley, L. Fraser, M. Bauer, N. Gormley, J. A. Gilbert, G. Smith, R. Knight,

641 Ultra-high-throughput microbial community analysis on the Illumina HiSeq and MiSeq

642 platforms. *ISME J.* (2012), doi:10.1038/ismej.2012.8.

643 29. E. Bolyen, J. R. Rideout, M. Dillon, N. Bokulich, C. Abnet, G. Al-Ghalith, H. Alexander,

644 E. Alm, M. Arumugam, F. Asnicar, Y. Bai, J. Bisanz, K. Bittinger, A. Brejnrod, C.

645 Brislawn, C. T. Brown, B. Callahan, A. M. Caraballo-Rodríguez, J. Chase, E. Cope, R. Da

646 Silva, P. Dorrestein, G. Douglas, D. Durall, C. Duvallet, C. Edwardson, M. Ernst, M.

647 Estaki, J. Fouquier, J. Gauglitz, D. Gibson, A. Gonzalez, K. Gorlick, J. Guo, B. Hillmann,

648 S. Holmes, H. Holste, C. Huttenhower, G. Huttley, S. Janssen, A. Jarmusch, L. Jiang, B.

649 Kaehler, K. Bin Kang, C. Keefe, P. Keim, S. Kelley, D. Knights, I. Koester, T. Kosciolek,

650 J. Kreps, M. G. Langille, J. Lee, R. Ley, Y.-X. Liu, E. Loftfield, C. Lozupone, M. Maher,

651 C. Marotz, B. Martin, D. McDonald, L. McIver, A. Melnik, J. Metcalf, S. Morgan, J.

652 Morton, A. T. Naimey, J. Navas-Molina, L. F. Nothias, S. Orchanian, T. Pearson, S.

653 Peoples, D. Petras, M. L. Preuss, E. Pruesse, L. B. Rasmussen, A. Rivers, M. Robeson, II,

654 P. Rosenthal, N. Segata, M. Shaffer, A. Shiffer, R. Sinha, S. J. Song, J. Spear, A.

655 Swafford, L. Thompson, P. Torres, P. Trinh, A. Tripathi, P. Turnbaugh, S. Ul-Hasan, J. J.

656 van der Hooft, F. Vargas, Y. Vázquez-Baeza, E. Vogtmann, M. von Hippel, W. Walters,

657 Y. Wan, M. Wang, J. Warren, K. Weber, C. H. Williamson, A. Willis, Z. Z. Xu, J.

Zaneveld, Y. Zhang, Q. Zhu, R. Knight, J. G. Caporaso, QIIME 2: Reproducible, interactive, scalable, and extensible microbiome data science. *PeerJ* (2018), doi:10.7287/peerj.preprints.27295.

30. B. J. Callahan, P. J. McMurdie, M. J. Rosen, A. W. Han, A. J. A. Johnson, S. P. Holmes, DADA2: High-resolution sample inference from Illumina amplicon data. *Nat. Methods* (2016), doi:10.1038/nmeth.3869.

31. N. A. Bokulich, B. D. Kaehler, J. R. Rideout, M. Dillon, E. Bolyen, R. Knight, G. A. Huttley, J. Gregory Caporaso, Optimizing taxonomic classification of marker-gene amplicon sequences with QIIME 2's q2-feature-classifier plugin. *Microbiome* (2018), doi:10.1186/s40168-018-0470-z.

32. D. McDonald, M. N. Price, J. Goodrich, E. P. Nawrocki, T. Z. Desantis, A. Probst, G. L. Andersen, R. Knight, P. Hugenholtz, An improved Greengenes taxonomy with explicit ranks for ecological and evolutionary analyses of bacteria and archaea. *ISME J.* (2012), doi:10.1038/ismej.2011.139.

33. J. Oksanen, F. G. Blanchet, M. Friendly, R. Kindt, P. Legendre, D. Mcglinn, P. R. Minchin, R. B. O'Hara, G. L. Simpson, P. Solymos, M. H. H. Stevens, E. Szoecs, H. Wagner, vegan: Community Ecology Package. R package version 2.4-2. *Community Ecol. Packag.* (2019).

34. T. Mohammadi, H. W. Reesink, C. M. J. E. Vandenbroucke-Grauls, P. H. M. Savelkoul, Optimization of real-time PCR assay for rapid and sensitive detection of eubacterial 16S ribosomal DNA in platelet concentrates. *J. Clin. Microbiol.* (2003), doi:10.1128/JCM.41.10.4796-4798.2003.

35. G. Wallner, R. Amann, W. Beisker, Optimizing fluorescent in situ hybridization with

rRNA□targeted oligonucleotide probes for flow cytometric identification of microorganisms. *Cytometry* (1993), doi:10.1002/cyto.990140205.

36. O. A. Alexeyev, I. Marklund, B. Shannon, I. Golovleva, J. Olsson, C. Andersson, I. Eriksson, R. Cohen, F. Elgh, Direct visualization of Propionibacterium acnes in prostate tissue by multicolor fluorescent in situ hybridization assay. *J. Clin. Microbiol.* (2007), doi:10.1128/JCM.01543-07.

37. J. Oh, A. L. Byrd, C. Deming, S. Conlan, H. H. Kong, J. A. Segre, B. Barnabas, R. Blakesley, G. Bouffard, S. Brooks, H. Coleman, M. Dekhtyar, M. Gregory, X. Guan, J. Gupta, J. Han, S. L. Ho, R. Legaspi, Q. Maduro, C. Masiello, B. Maskeri, J. McDowell, C. Montemayor, J. Mullikin, M. Park, N. Riebow, K. Schandler, B. Schmidt, C. Sison, M. Stantripop, J. Thomas, P. Thomas, M. Vemulapalli, A. Young, Biogeography and individuality shape function in the human skin metagenome. *Nature* (2014), doi:10.1038/nature13786.

**Acknowledgments:** We thank all members of the Gitai lab for their insights and comments. We also thank Dr. Gary Laevsky and the Princeton Molecular Biology Microscopy Core, which is a Nikon Center of Excellence, for microscopy support; Dr. Wei Wang and the Genomics Core Facility in The Lewis Sigler Institute for Integrative Genomics at Princeton University for support with 16S rRNA gene amplicon sequencing; Matthew Cahn and Jaime Lopez for their assistance with processing 16S rRNA gene amplicon sequencing data; Bahar Javdan for processing the human fecal sample; and Elizabeth Grice for support and feedback. **Funding:** Funding was provided in part by NIH (DP1AI124669 to Z.G., E.M.A., and B.P.B., and T32 GM007388 to E.M.A). Additional funding provided by the National Science Foundation (NSF PHY-1734030 to B.P.B.). Research reported in this publication was also supported by the National Center for Advancing Translational Sciences of the National Institutes of Health under Award Number TL1TR003019 (E.M.A) and by the Schmidt Transformative Technology Fund (E.M.A.). This work was supported in part by the Penn Skin Biology and Diseases Resource-based Center (P30-AR068589). The contents are solely the responsibility of the authors and do not necessarily represent the official views of the respective funding agencies.

**Author contributions:** Conceptualization, Z.G., E.M.A., and D.D.; Methodology, Z.G., E.M.A., and D.D.; Software, E.M.A. and B.P.B.; Formal Analysis, E.M.A. and B.P.B.; Investigation, E.M.A., K.A.L., and X.M.; Resources, Z. G., D.D., and A.P.; Writing – Original Draft, Z.G. and E.M.A.; Writing – Reviewing & Editing, Z.G., E.M.A., B.P.B., D.D., and A.P.; Visualization, E.M.A. Z.G., and B.P.B.; Supervision, Z.G., D.D., and A.P.; Funding Acquisition, Z.G.

**Competing interests:** Authors declare no competing interests.

719

720 **Materials and correspondence:** All data is available in the main text or the supplementary

721 materials. Additionally, the raw data that support the findings of this study are available from the

722 corresponding author upon request (Zemer Gitai, zgitai@princeton.edu).

723

## Supplementary information

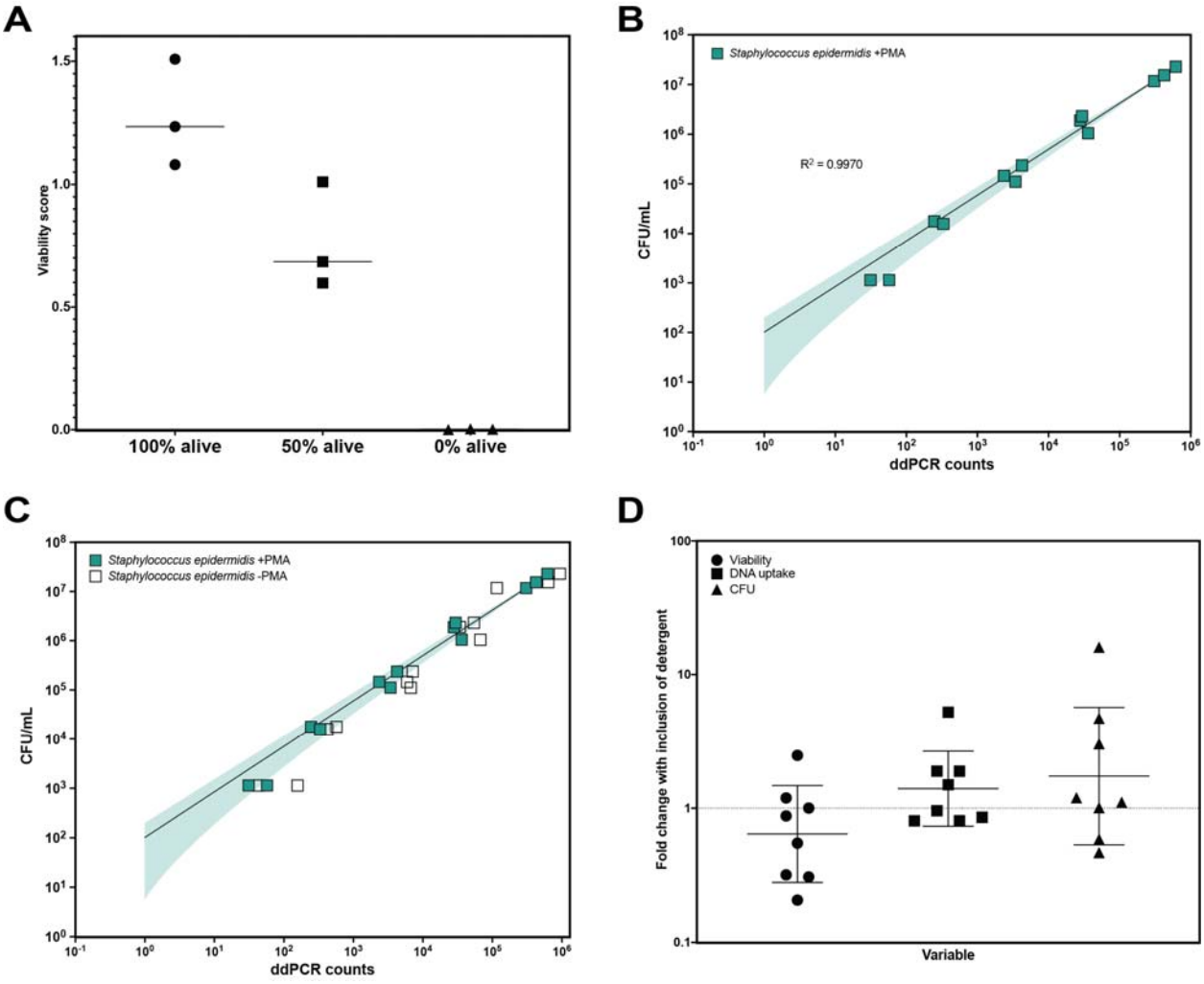


**Fig. S1.** PMA and sampling controls. (A) PMA-ddPCR validation controls on known ratios of heat-killed and exponentially-growing *E. coli* cultures. PMA-ddPCR performed on a population of exponentially-growing cells resulted in a viability score slightly above 1.0 (1.23), which was likely due to continued bacterial growth during the experiment. PMA-ddPCR performed on a population of 100% heat-killed cells resulted in a viability score of 0. Populations consisting of 50% (by volume) heat-killed and 50% exponentially-growing cells exhibited an average viability score of 0.69. (B) Standard curve showing correlation between PMA-ddPCR counts and CFU for exponentially-growing *Staphylococcus epidermidis*. 95% confidence interval is shown in the green shaded region. (C) The same standard curve as shown in (B) with the addition of *S.*

735 *epidermidis* that was not treated with PMA. (D) The effect of including 0.1% Triton X100 in

736 swabbing buffer used for skin microbiome sampling.

737

738

739

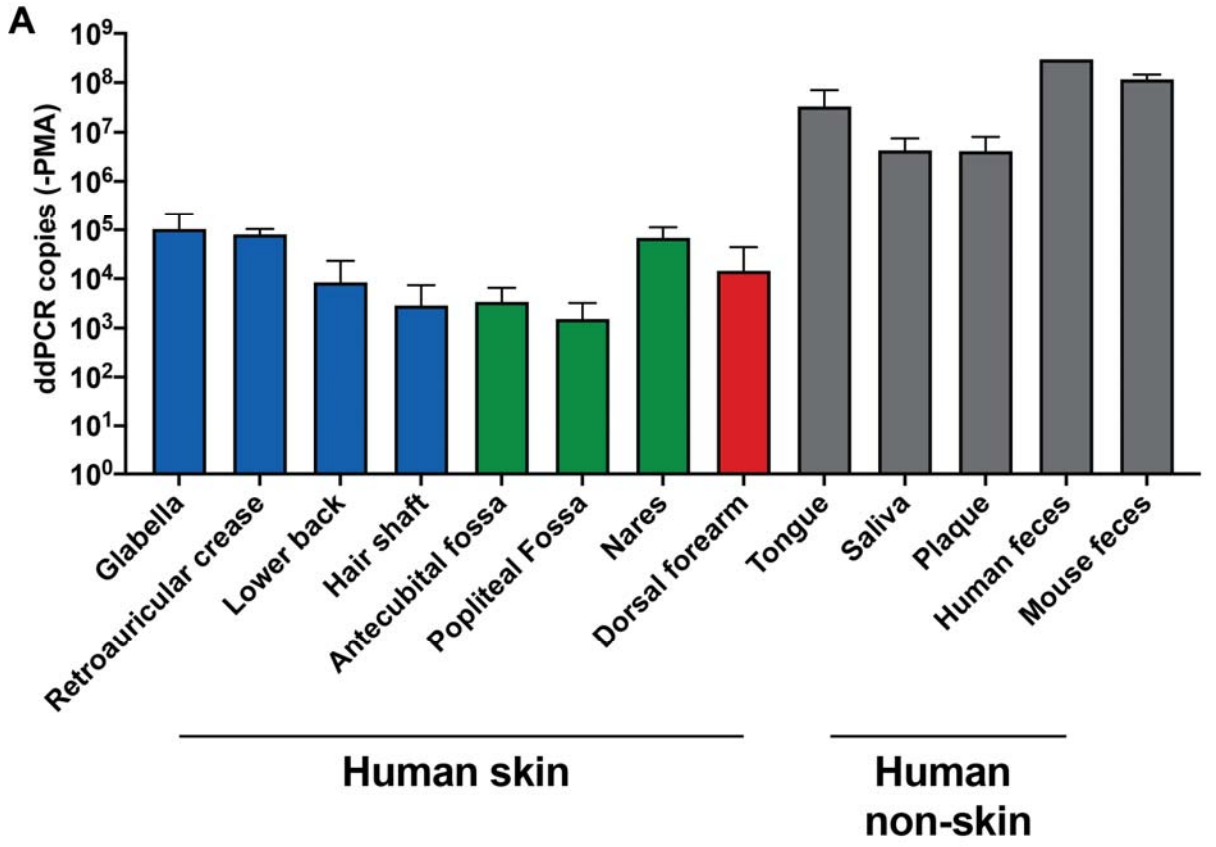


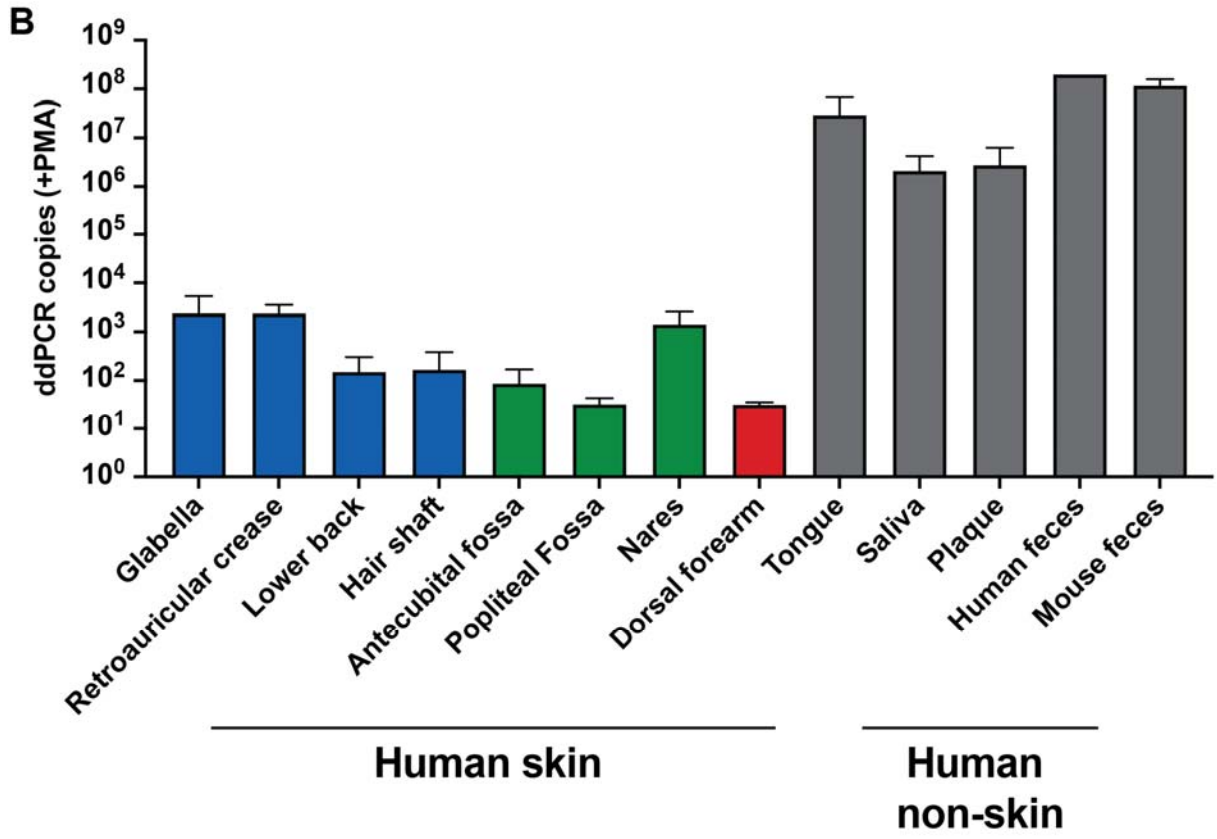

741 **Fig. S2.** Copies per 20 µL ddPCR reaction without (A) and with (B) the use of PMA. These data

742 were used to calculate the viability score shown in Fig. 2.

743

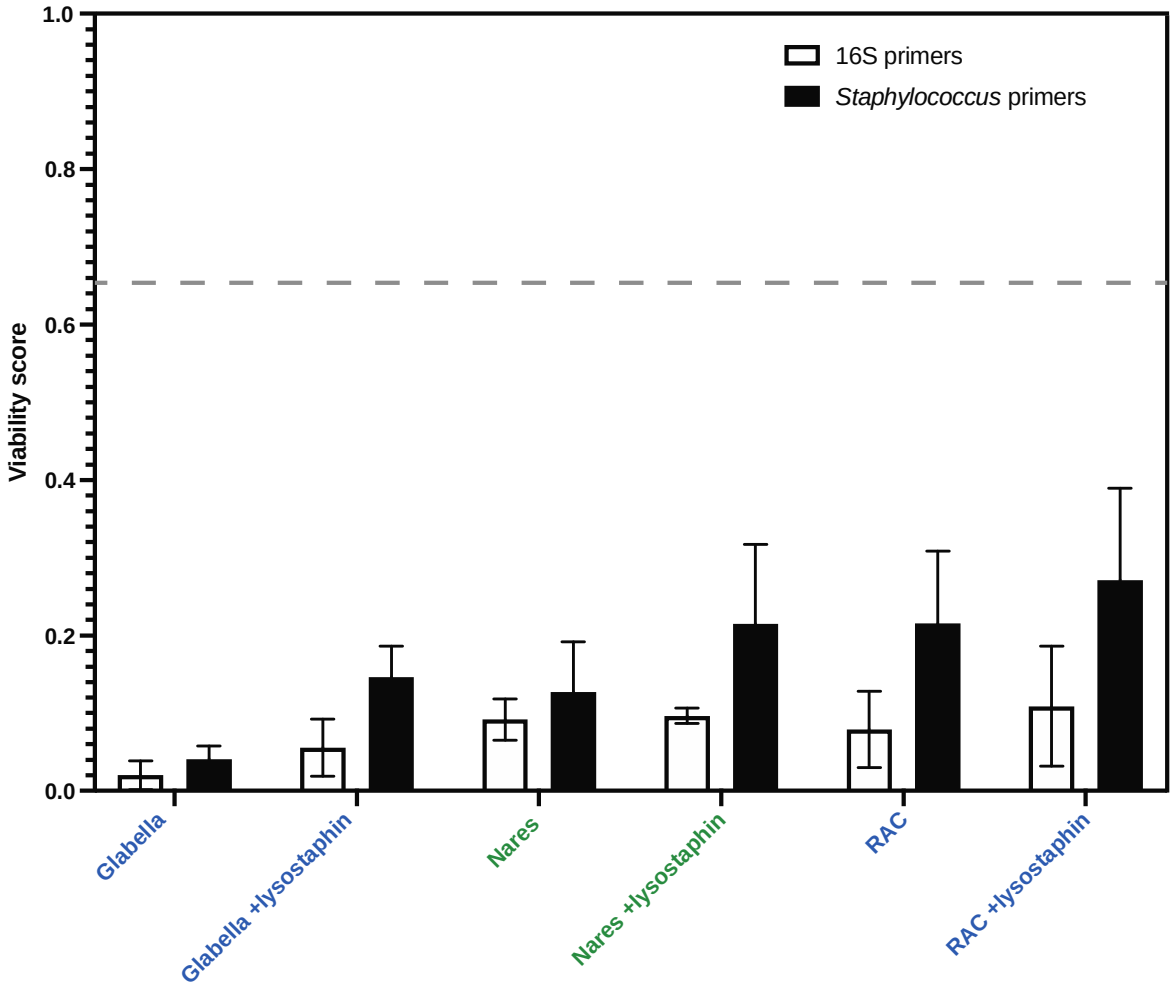


**Fig. S3.** Viability score for three skin sites using lysostaphin and *Staphylococcus*-specific PCR primers. The three skin sites with the most abundant bacterial DNA are shown. Half of each sample was treated with lysostaphin prior to DNA isolation to assess how the viability score would change. ddPCR was performed on each sample using both 16S primers (white bars) and *Staphylococcus*-specific (black bars) primers. The dashed line indicates the average viability score of non-skin microbiome sites (0.66). N=3 for all.

| **Name** | **Description** | **Sequence (5' - 3')** | **Reference** |
|---|---|---|---|
| | ddPCR FP (Universal bacterial 16S qPCR FP) | TCCTACGGGAGGCAGCAGT | (*34*) |
| | ddPCR RP (Universal bacterial 16S qPCR RP) | GGACTACCAGGGTATCTAATCCTGTT | (*34*) |
| EFTU_FP | Staph-specific ddPCR forward primer | ATGCCACAAACTCGTGAACA | this paper |
| EFTU_RP | Staph-specific ddPCR reverse primer | ACATCGTCACCTGGGAAGTC | this paper |
| EUB338 | Pan-bacterial FISH probe | GCTGCCTCCCGTAGGAGT | (*17*) |
| NonEUB338 | Nonsense control FISH probe | CGACGGAGGGCATCCTCA | (*35*) |
| | C. acnes FISH probe | GAGTGTGTGAACCGATCATGTAGTAGGCAA | (*36*) |
| 27F | Forward 16S sequencing primer | AGAGTTTGATCCTGGCTCAG | (*37*) |
| 534R | Reverse 16S sequencing primer | ATTACCGCGGCTGCTGG | (*37*) |

752 **Table S1.** Nucleotide sequences used in this study.

753